Finite-Time Fault-Tolerant Integrated Motion Control for Autonomous Vehicles With Prescribed Performance

Tenglong Huang, Jue Wang, Huihui Pan, *Member, IEEE*, and Weichao Sun, *Senior Member, IEEE*

***Abstract*— Vehicle-integrated motion control (IMC) with the capability to enhance the overall performance by considering the couplings and interactions among various subsystems is an active and open issue. This article proposes a novel finite-time lateral and longitudinal IMC scheme to bypass the resulting complex nonlinearities on the basis of time-delay estimation (TDE). The precise tracking of reference trajectory is achieved where the transient errors are limited to the designed prescribed performance functions (PPFs). The expected steady-state region can be entered in a fixed time, and then the state errors convergence to zero asymptotically. Meanwhile, actuator faults and external disturbance, for autonomous vehicles (AVs) equipped with abundant actuators, are frequently encountered in practice. The presented controller incorporating fault-tolerant ability and disturbance rejection is implemented to further optimize the robustness and reliability. In particular, no auxiliary approximate mechanism or additional prior knowledge is needed. The simulation results for standard maneuvers and planned trajectory tracking are conducted to demonstrate the benefits of the constructed integrated control scheme, in terms of tracking performance (position tracking error dropped over 70%), handling (yaw rate tracing error dropped over 10%), and stability (vehicle sideslip angle dropped over 70%).**

***Index Terms*— Autonomous vehicles (AVs), fault tolerant, integrated motion control (IMC), prescribed performance, time-delay estimation (TDE).**

I. Introduction

AUTONOMOUS vehicles (AVs) [1], [2] have great potential to reduce traffic congestion, energy consumption, and greenhouse gas emission caused by the traditional fossil fuel vehicles. These advantages motivate the burgeoning interest and rapid technological progress in this field, for example, the novel and effective low-cost control method proposed in [3]. From a technical perspective, the AVs are mainly composed of environment perception, motion planning, and motion control [4], [5], [6]. The motion control module generates command control signals and directly affects the overall performance, which is one of the key technical challenges of the AVs.

To handle this issue and attain superior dynamic properties, there have been several practical applications in Level 1 or Level 2 [4] AVs. For instance, the anti-lock braking system (ABS) [7], direct yaw moment control (DYC) [8], and active suspension system (ASS) are employed to optimize the dynamic performance of longitudinal, lateral, and vertical subsystems, respectively. In practice, when various vehicle subsystems work simultaneously, the interactions and conflicts are inevitable. An efficient countermeasure to cope with the induced performance degradation is the integrated vehicle motion control [9], [10]. Due to the dynamical model complexity and nonlinearity, multiple subsystems integrated control can be an arduous task, and this question has not been studied sufficiently so far [11]. Compared with the most results, assume longitudinal speed is constant to simplify [12], the integrated lateral and longitudinal motion control with time-varying longitudinal velocity is investigated in this article.

Optimization-based methodology [9] offers an attractive and feasible candidate for integrated control by the designed bottom-to-top scheme. In addition, the adaptive control framework is established in [13], which coordinates the active front steering and DYC to enhance the vehicle stability. In contrast to asymptotically stable strategies mentioned above, terminal sliding-mode control (TSMC) [14] assures faster finite-time convergence property for vehicles. It is noteworthy reminding that non-singular terminal sliding mode (NTSM) [15] is established to address the singularity phenomenon for conventional TSMC. However, the settling time of the finite-time control methodologies is dependent on the initial states. Correspondingly, the fixed time control approaches introduced in [16] are capable of overcoming the dependence effectively. The fixed time convergence property for AVs contributes to quickly track the replanned trajectories generated in real-time by higher level motion planning algorithms to ensure collision-free. In addition, transient response is another crucial aspect of AVs. In practice, the transient response can be constrained to a safe range by considering the vehicle characteristics, which is more realistic than assuming that the trajectory is accurately tracked with

Manuscript received 15 September 2022; revised 1 November 2022; accepted 12 December 2022. Date of publication 26 December 2022; date of current version 13 September 2023. This work was supported in part by the National Natural Science Foundation of China under Grant U1964201, Grant 62173108, and Grant 62022031; in part by the Post-Doctoral Science Foundation under Grant 2019T120270 and Grant LBH-TZ2111; in part by the Major Scientific and Technological Special Project of Heilongjiang Province under Grant 2021ZX05A01; and in part by the Fundamental Research Funds for the Central Universities under Grant HIT.OCEF.2022012. *(Corresponding author: Huihui Pan.)*

Tenglong Huang, Jue Wang, and Weichao Sun are with the Research Institute of Intelligent Control and Systems, Harbin Institute of Technology, Harbin 150001, China (e-mail: huangtenglong@hit.edu.cn; juewang@hit.edu.cn; w.sun@hit.edu.cn).

Huihui Pan is with the Research Institute of Intelligent Control and Systems and Robot Innovation Center Company Ltd., Harbin Institute of Technology, Harbin 150001, China (e-mail: huihuipan@hit.edu.cn).

Digital Object Identifier 10.1109/TTE.2022.3232521

zero error. Wang et al. [17] provide a theoretically guaranteed solution for nonlinear systems subject to transient behavior constraints, by utilizing the presented error transformation. Hereafter, a rich body of relevant pioneering results emerged in the areas of car-like mobile robots [18], vehicle suspension, and robot manipulators [19]. Nonetheless, to the authors' knowledge, there are no results that focus on tackling transient constraints, steady-state performance, interactions, and coupling for AVs integrated control concurrently.

Once the strong coupling is taken into consideration, the physics-based vehicle model is highly nonlinear and cannot be constructed precisely. Neural network (NN) is exploited to identify the vehicle dynamics characteristics in [20], and the learned model can even surpass the performance of the physics-based model. The adaptive dynamic programming technique is a model-free alternative that allows optimizing the vehicle lateral stability [21]. Nevertheless, one common downside of these techniques is the need for excessive collected data. To circumvent this, the inspiration for the approach devised in this article is drawn from the time-delay estimation (TDE) technology [22]. TDE approximates the nonlinear plant model by means of the time-delay information, which overcomes the expensive computational burden of the aforementioned learning methods.

AVs are equipped with numerous electro actuators [23], [24] to accomplish the demanded driving, braking, and steering. Correspondingly, AVs can be modeled as under-actuated [25], fully actuated, and over-actuated [26]. This article focuses on fully actuated vehicle motion control. Actuator faults [27], [28], involving additive faults and loss-of-effectiveness faults, appear naturally owing to the flux linkage, mechanical wear, and aging, which can deteriorate the vehicle handling, stability, and so on. Meanwhile, unknown disturbances intrinsically exist in real systems, which can also deteriorate the control performance dramatically. NN and observer [29] are valuable tools to estimate and deal with the occurred disturbances and faults. As in [30] and [18], the uncertainties and disturbances for car-like mobile robots can be effectively compensated by employing the designed new NN approximator, which contributes to increase the robustness. Despite this, observer design and approximate structure construction are notable problems in themselves. The ability of TDE without auxiliary mechanisms to accommodate the actuator faults and disturbances has been validated in [31]; however, in which the known upper boundness is necessary.

Inspired by the previous discussion, devising an integrated lateral and longitudinal motion control framework for AVs to track the reference trajectory and dynamics with faster convergence is the primary objective of this article. Besides, the transient response constraints, steady-state requirements, unknown disturbances, and actuator faults are addressed to achieve superior overall performance and robustness. More in detail, the contributions of this article are given below.

1) A finite-time integrated motion control (IMC) scheme with time-varying longitudinal velocity is presented to address the interactions and coupling between lateral and longitudinal dynamics. Moreover, the proposed control framework bridges the gap between vehicle dynamics control [9] and trajectory tracking [32] for AVs. Integrated dynamics control can be transformed as a trajectory tracking problem by employing the desired signal generation approach, which both be unified and handled with the designed controller.
2) The desired trajectory and dynamics can be tracked accurately with fast response. Specifically, the transient tracking error is restricted by the prescribed performance function (PPF). Another distinguishing aspect of the integrated controller is that it ensures the trajectory tracking errors enter the prescribed steady-state precision region in a fixed time. Subsequently, the asymptotic convergence of the state errors is asserted.
3) Furthermore, the negative impacts of the unknown external disturbance and actuator faults are eliminated. Although the ability of NTSM to reject disturbance has been revealed in the literature, performance declines unavoidably when actuator faults occur. Toward this end, TDE is embedded to enhance robustness and reliability against actuator faults. Note that no additional boundness information and approximate tools are required.

II. Problem Statement

In this section, the mathematical models of vehicle are introduced to shed a clear light on the couplings and interactions between the longitudinal and lateral subsystems. Moreover, the trajectory tracking problem transformed from the reference dynamics signals is stated to highlight the control object.

A. Vehicle Model

The kinematic model [33] of the autonomous ground vehicle is described as

$$\dot{\eta} = H(\phi)\upsilon \tag{1}$$

where the velocity vector $\upsilon = [\upsilon_x, \upsilon_y, \omega]^{\mathrm{T}}$ in the vehicle frame-fixed axes consists of longitudinal velocity υ_x, lateral velocity υ_y, and yaw rate ω. $\eta = [x, y, \phi]^{\mathrm{T}}$ is composed of global position (x, y) and yaw angle ϕ. $H(\phi) = [\cos\phi \ -\sin\phi \ 0; \sin\phi \ \cos\phi \ 0; \ 0 \ 0 \ 1]$ denotes the rotation matrix.

The wheel rotational dynamics $\dot{\gamma}$ [9] are given by

$$I\dot{\gamma}_{ij} = -R_{\text{eff}}F_{xij} + T_{ij} \tag{2}$$

where the subscription $i \in \{f, r\}$ represents the front or rear wheel, and $j \in \{l, r\}$ represents the left or right wheel. F_{xij}, T_{ij}, R_{eff}, and I are the corresponding wheel driving force, torque, rolling radius, and moment of inertia, respectively. Steering angle input is denoted by δ, and the vector $\tau_d := [\tau_{d1}, \tau_{d2}, \tau_{d3}]^{\mathrm{T}}$ is defined as $\tau_{d1} = T_{fl}\cos\delta + T_{rl}$, $\tau_{d2} = T_{fr}\cos\delta + T_{rr}$, and $\tau_{d3} = \delta$. Then, the longitudinal, lateral,

and yaw dynamics [21], [33], [34], [35] of AVs have the form

$$\begin{cases} \dot{v}_x = v_y\omega - \dfrac{C_a}{m}v_x^2 + \dfrac{1}{mR_{\text{eff}}}(\tau_{d1}+\tau_{d2}) - u_{\ell 1} + u_{\text{dist1}} \\ \dot{v}_y = -\dfrac{(C_f+C_r)v_y}{mv_x} + \left(\dfrac{C_r l_r - C_f l_f}{mv_x} - v_x\right)\omega + \dfrac{C_f}{m}\tau_{d3} \\ \qquad + u_{\ell 2} + u_{\text{dist2}} \\ \dot{\omega} = \dfrac{(C_r l_r - C_f l_f)v_y - \left(C_f l_f^2 + C_r l_r^2\right)\omega}{I_z v_x} + \dfrac{C_f l_f}{I_z}\tau_{d3} \\ \qquad - \dfrac{l_s}{I_z R_{\text{eff}}}(\tau_{d1}-\tau_{d2}) + u_{\ell 3} + u_{\text{dist3}} \end{cases} \tag{3}$$

where the vehicle parameters [9] of a Hatchback vehicle used in this article are reported in Fig. 1 and Table I. The complex dynamics are unnecessary for the controller design, which is used as the plant to evaluate the proposed controller. $u_\ell := [u_{\ell 1}, u_{\ell 2}, u_{\ell 3}]^{\text{T}}$ and $u_{\text{dist}} := [u_{\text{dist1}}, u_{\text{dist2}}, u_{\text{dist3}}]^{\text{T}}$ refer to the unmodeled terms of AVs [33] and external disturbance, respectively. Consider the virtual control input $\tau := [\tau_1, \tau_2, \tau_3]^{\text{T}}$ is defined as

$$\begin{cases} \tau_1 = \dfrac{1}{mR_{\text{eff}}}(\tau_{d1}+\tau_{d2}) \\ \tau_2 = \dfrac{C_f}{m}\tau_{d3} \\ \tau_3 = \dfrac{C_f l_f}{I_z}\tau_{d3} - \frac{l_s}{I_z R_{\text{eff}}}(\tau_{d1}-\tau_{d2}). \end{cases} \tag{4}$$

The vector τ_f with the loss-of-effectiveness faults $\mathcal{L}_a := \text{diag}(\ell_{a1}(t), \ell_{a2}(t), \ell_{a3}(t))$ and bias faults $z_a := [z_{a1}(t), z_{a2}(t), z_{a3}(t)]^{\text{T}}$ [27], [36], [37] can be represented as

$$\tau_f = \mathcal{F}(L_a\tau_d + z_a) \tag{5}$$

where the known constant conversion matrix $\mathcal{F} := [(1/mR_{\text{eff}})\ (1/mR_{\text{eff}})\quad 0; 0\ 0\ (C_f/m); -(l_s/(I_z R_{\text{eff}}))(l_s/(I_z R_{\text{eff}}))\ (C_f l_f/I_z)]$ is invertible. The loss-of-effectiveness coefficient $0 < \ell_{ai} \le 1, i = 1, 2, 3$. The impact of actuator faults on vehicle systems can be observed in (3) and (5).

Remark 1: Actuator faults are common for vehicles equipped with numerous actuators [27]. For example, the harmonics flux linkage can be modeled as the bias faults [26]. The loss-of-effectiveness faults caused by mechanical wear and aging can be represented as efficiency factor $\mathcal{L}_a$. Actuator faults for AVs are detailed in [27] and [38], where the unknown actuator faults (5) are considered and handled in this article.

Summarizing, when considering actuator failures and unknown external disturbance u_{dist}, the dynamics model of the vehicle can be expressed by the following system:

$$\dot{\eta} = H(\phi)v \tag{6}$$

$$\dot{v} = J(v)v + u_\ell + \tau_f + u_{\text{dist}} \tag{7}$$

where J as shown in the equation at the bottom of the page.

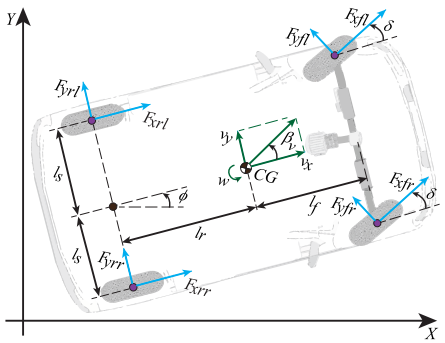

Fig. 1. Schematic of the vehicle model. CG represents the center of gravity for the AV.

TABLE I
VEHICLE PARAMETERS

Notation	Description	Value(Unit)
C_f/C_r	Front/Rear Cornering Stiffness	$22010N/rad$
C_a	Aerodynamic Drag Coefficient	$0.005N \cdot s^2/m^2$
l_f	Length between Front Axle and CG	$1.04m$
l_r	Length between Rear Axle and CG	$1.56m$
l_s	Half Wheel Track	$0.74m$
I_z	Yaw Moment of Inertial	$1343.1kg \cdot m^2$
m	The Mass of Vehicle	$1110kg$
k_{swa}	Steering Wheel Angle Coefficient	0.02
R_{eff}	The Rolling Radius of Wheel	$0.31m$

Remark 2: It is worth mentioning that this article focuses on vehicle lateral and longitudinal IMC, namely the lateral, longitudinal, and yaw dynamics are taken into consideration. The roll, pitch, and vertical dynamics of the vehicle chassis are ignored in this article.

B. Problem Formulation

To bridge the gap between vehicle dynamics control and trajectory tracking for AVs, the above system can be recast as

$$\dot{\eta} = \psi \tag{8}$$

$$\dot{\psi} = \mathcal{M}(\eta, \psi, t) + H(\psi)\tau + \mathcal{O}(\eta, \psi, t) \tag{9}$$

where the vector $\psi := [\psi_1, \psi_2, \psi_3]^{\text{T}}$ is the vehicle velocity in the global coordinate frame, $\mathcal{M} := \mathcal{Q}(\psi)\psi + H(\psi)J(\eta, H^{\text{T}}\psi)H^T\psi$, $\mathcal{Q}(\omega) := [0\ -\omega\ 0; \omega\ 0\ 0; 0\ 0\ 0]$, and $\mathcal{O} := H(\psi)(u_\ell + u_{\text{dist}} + \tau_f - \tau)$.

Calculating the desired trajectory $\eta_d := [x_d, y_d, \phi_d]^{\text{T}}$ according to reference vehicle dynamics $v_d := [v_{xd}, v_{yd}, \omega_d]^{\text{T}}$, we obtain that

$$\dot{\eta}_d = H(\phi_d)v_d. \tag{10}$$

Using these definitions, the tracking error vector $e \in \mathbb{R}^3$ can be derived as

$$e = \eta - \eta_d. \tag{11}$$

$$J = \left[\frac{-v_x C_a}{m}\ \omega\ 0;\quad 0 - \frac{C_f + C_r}{mv_x}\ \frac{C_r l_r - C_f l_f}{mv_x} - v_x;\quad 0\ \ \frac{C_r l_r - C_f l_f}{v_x I_z}\ \frac{-C_r l_r^2 - C_f l_f^2}{v_x I_z}\right].$$

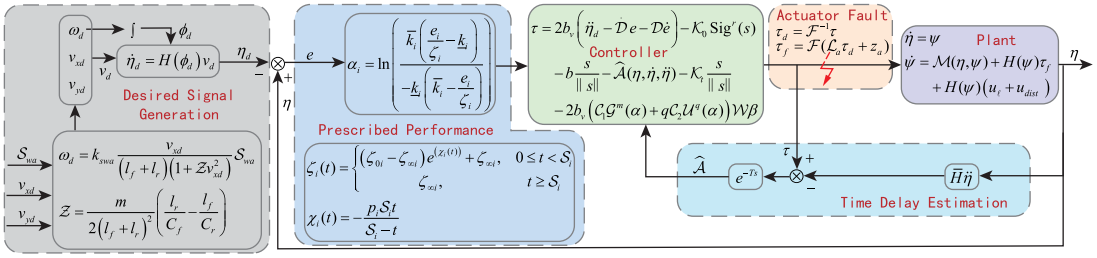

Fig. 2. Block diagram of the devised integrated fault-tolerant motion control scheme.

The primary purpose of this article is to develop an integrated control framework to handle the couplings and interactions between the longitudinal and lateral subsystems. As mentioned above, the vehicle-integrated dynamics control can be converted into a trajectory tracking problem. For example, the two problems can be handled with a unified control approach. In addition to accurate trajectory tracking, faster fixed-time convergence and superior transient performance satisfying the prescribed constraints are also expected. Meanwhile, for the sake of enhancing robustness and reliability, external disturbances and actuator failures are taken into account.

Lemma 1 [39]: Let $\upsilon_1, \upsilon_2, \ldots, \upsilon_n \geq 0, \gamma > 1$. The following inequality holds $\sum_{i=1}^{n} \upsilon_i^{\gamma} \geq n^{1-\gamma} (\sum_{i=1}^{n} \upsilon_i)^{\gamma}$.

Lemma 2 [40]: Consider the system $\dot{\eta} = g(\eta), \eta(0) = \eta_0, \eta \in \mathbb{R}^n$. Let $\varpi, \mu > 0, \beta > 1, \alpha \in (0, 1)$. If the positive-definite and continuous radially unbounded function $\mathcal{V} : \mathbb{R}^n \to \mathbb{R}^+$ exists such that $\dot{\mathcal{V}}(\eta) \leq -\varpi \mathcal{V}(\eta)^{\alpha} - \mu \mathcal{V}(\eta)^{\beta}$ holds, the system is fixed-time stable with settling time satisfying $\mathcal{B} \leq \frac{1}{\varpi(1-\alpha)} + \frac{1}{\mu(\beta-1)}$.

Assumption 1: The nonlinear components $\mathcal{M}(\eta, \psi, t)$, $H(\psi)$, and $\mathcal{O}(\eta, \psi, t)$ in the vehicle model (9) are continuous or discontinuous but bounded by unknown boundaries. It is reasonable for the vehicle chassis control system in practice.

Remark 3: The designed controller in this article is intended to track the safe collision-free desired trajectory generated by the motion planning and be embedded in the Levels 1–5 AVs as a sub-module. As detailed in [4] and [5], it is clear that the controller can be easily introduced into Levels 1–5 AVs, including urban or highway driving scenarios, etc., as a lower-level module for decision-making and motion planning, when the controller can track the desired motion accurately.

III. Control Scheme

This section is devoted to describing the developed integrated longitudinal and lateral fault-tolerant motion control framework, which is depicted in Fig. 2. More precisely, the reference values of the integrated vehicle dynamics can be obtained using the desired signal generation module. The tracking error is calculated by combining the real-time state, which is transformed to obtain the desired convergence properties by means of a PPF. The time-delay information removes the need for complex lateral–longitudinal dynamics coupling relationships in the controller design, which can be seen from the resulting controller. More details are provided below.

A. Desired Signal Generation

The desired longitudinal velocity υ_{xd} can be set arbitrarily to meet the need of driver. The desired yaw rate ω_d can be derived from input steering wheel angle $\mathcal{S}_{wa}$ [9], [21], which is described as

$$\omega_d = k_{swa} \frac{\upsilon_{xd}}{(l_f + l_r)(1 + \mathcal{Z}\upsilon_{xd}^2)} \mathcal{S}_{wa} \tag{12}$$

where

$$\mathcal{Z} = \frac{m}{2(l_f + l_r)^2} \left(\frac{l_r}{C_f} - \frac{l_f}{C_r} \right). \tag{13}$$

With the aim of enhancing stability, this article sets as $\upsilon_{yd} = 0$. Correspondingly, the reference trajectory can be calculated using (10).

B. Time Delay Estimation

Considering $\dot{\psi} = \ddot{\eta}$ and (9) yield

$$H^{\mathrm{T}}(\psi)\ddot{\eta} = H^{\mathrm{T}}(\psi)\ \mathcal{M}(\eta, \dot{\eta}) + \tau + H^{\mathrm{T}}\mathcal{O} \tag{14}$$

or equivalently

$$\bar{H}\ddot{\eta} = \mathcal{A}(\eta, \dot{\eta}, \ddot{\eta}) + \tau \tag{15}$$

where $\mathcal{A}(\eta, \dot{\eta}, \ddot{\eta}) = (-H^{\mathrm{T}}(\psi) + \bar{H})\ddot{\eta} + H^{\mathrm{T}}(\psi)\mathcal{M}(\eta, \dot{\eta}) + H^{\mathrm{T}}\mathcal{O}$, $\bar{H} := 2b_v * I_3$, b_v is a const, and the 3×3 identity matrix is indicated by I_3. Time-delay information [22], without the need of any prior knowledge about the vehicle model, is leveraged to estimate the system model in the form

$$\hat{\mathcal{A}}(\eta, \dot{\eta}, \ddot{\eta}) = \mathcal{A}(\eta, \dot{\eta}, \ddot{\eta})_{t-T} \tag{16}$$

where T is the time-delay constant. Recalling (15), we obtain

$$\mathcal{A}(\eta, \dot{\eta}, \ddot{\eta})_{t-T} = \tau_{t-T} - \bar{H}\ddot{\eta}_{t-T}. \tag{17}$$

Therefore, the TDE reads

$$\mathcal{A}(\eta, \dot{\eta}, \ddot{\eta})_{t-T} = \tau_{t-T} - 2b_v\ddot{\eta}_{t-T}. \tag{18}$$

Hence, the estimation error vector ϱ is calculated as

$$\varrho = \mathcal{A}(\eta, \dot{\eta}, \ddot{\eta}) - \mathcal{A}(\eta, \dot{\eta}, \ddot{\eta})_{t-T}. \tag{19}$$

Obviously, ϱ is bounded when the plant (9) is continuous or bounded as Assumption 1 stated, and the time delay T is a short period of time. For example, there exists an unknown bounded constant ι, such that $|\varrho| < \iota$, where the boundness information ι is unnecessary. Thus, a diagonal parameter matrix $\mathcal{K}_t$ satisfying

$$\{\mathcal{K}_t\}_{ii} > \iota_i, \quad i = 1, 2, 3 \tag{20}$$

also exists and can be obtained by trial-and-error, which has been proven in the previous studies [22], [41] and widely used in the literature. Recalling (15), the vehicle model represented by TDE can be rewritten as

$$\bar{H}\ddot{\eta} = \hat{\mathcal{A}}(\eta, \dot{\eta}, \ddot{\eta}) + \varrho + \tau. \tag{21}$$

C. Controller Design

To obtain superior transient performance, PPF methodology [17] is modified and introduced into the proposed control scheme in which the transient error $e_i(t), i = 1, 2, 3$ is constrained by the constructed prescribed function, namely

$$\underline{k}_i\zeta_i(t) < e_i(t) < \bar{k}_i\zeta_i(t) \tag{22}$$

where the constant $\mu_i \in (0, 1)$, and the performance coefficients $\underline{k}_i$ and $\bar{k}_i$ are chosen as follows:

$$\underline{k}_i = \begin{cases} -\mu_i, & e_i(0) \geq 0 \\ -1, & e_i(0) < 0 \end{cases}, \quad \bar{k}_i = \begin{cases} 1, & e_i(0) \geq 0 \\ \mu_i, & e_i(0) < 0. \end{cases}$$

It means that

$$\begin{cases} -\mu_i\zeta_i(t) < e_i(t) < \zeta_i(t), & e_i(0) \geq 0 \\ -\zeta_i(t) < e_i(t) < \mu_i\zeta_i(t), & e_i(0) < 0 \end{cases} \tag{23}$$

where

$$\zeta_i(t) = \begin{cases} (\zeta_{0i} - \zeta_{\infty i})e^{(\chi_i(t))} + \zeta_{\infty i}, & 0 \leq t < \mathcal{S}_i \\ \zeta_{\infty i}, & t \geq \mathcal{S}_i \end{cases} \tag{24}$$

$$\chi_i(t) = -\frac{p_i\mathcal{S}_i t}{\mathcal{S}_i - t} \tag{25}$$

and $\zeta_{\infty i}, \zeta_{0i}, \mathcal{S}_i$, and p_i are selected manually which satisfy $|e_i(0)| \in (\zeta_{\infty i}, \zeta_{0i})$, $\mathcal{S}_i > 0$, and $p_i > 1$. To proceed, the derivatives of $\chi_i(t)$ and smooth function $\zeta_i(t)$ [19] are

$$\dot{\zeta}_i(t) = \begin{cases} (\zeta_{0i} - \zeta_{\infty i})\dot{\chi}_i(t)e^{(\chi_i(t))}, & 0 \leq t < \mathcal{S}_i \\ 0, & t \geq \mathcal{S}_i \end{cases} \tag{26}$$

$$\dot{\chi}_i(t) = -\frac{p_i\mathcal{S}_i^2}{(\mathcal{S}_i - t)^2}. \tag{27}$$

The error e is mapped into the auxiliary unconstrained one σ by the constructed error transformation as follows:

$$\sigma(e) = \ln\left(\frac{\bar{k}_i(e - \underline{k}_i)}{-\underline{k}_i(\bar{k}_i - e)}\right). \tag{28}$$

Furthermore, the inverse mapping and derivative $\rho(e) := \dot{\sigma}(e)$ can be computed as

$$\sigma^{-1}(e) = \frac{\underline{k}_i\bar{k}_i(\exp(e) - 1)}{\underline{k}_i\exp(e) - \bar{k}_i}, \quad \rho(e) = \frac{1}{e - \underline{k}_i} + \frac{1}{\bar{k}_i - e} \tag{29}$$

then, the transformed error $\alpha_i := \sigma(e_i/\zeta_i)$ and its derivative as

$$\alpha_i = \ln\left(\frac{\bar{k}_i\left(\frac{e_i}{\zeta_i} - \underline{k}_i\right)}{-\underline{k}_i\left(\bar{k}_i - \frac{e_i}{\zeta_i}\right)}\right) \tag{30}$$

$$\dot{\alpha}_i = \varpi_i(\dot{e}_i + \theta_i e_i) \tag{31}$$

where

$$\varpi_i = \frac{1}{e_i - \zeta_i\underline{k}_i} + \frac{1}{\zeta_i\bar{k}_i - e_i}, \quad \theta_i = -\frac{\dot{\zeta}_i}{\zeta_i}. \tag{32}$$

Defining $\mathcal{D} := \text{diag}(\theta_1, \theta_2, \theta_3)$ and $\mathcal{W} := \text{diag}(\varpi_1, \varpi_2, \varpi_3)$, (30) is converted to a vector form as

$$\dot{\alpha} = \mathcal{W}(\dot{e} + \mathcal{D}e).$$

For convenience, let $\beta := \dot{e} + \mathcal{D}e$, we get

$$\dot{\beta} = \ddot{e} + \dot{\mathcal{D}}e + \mathcal{D}\dot{e} \tag{33}$$

$$\dot{\alpha} = \mathcal{W}\beta. \tag{34}$$

The following sliding function is established:

$$s = \mathcal{C}_1\mathcal{N}^m(\alpha) + \mathcal{C}_2\text{Sig}^q(\alpha) + \beta \tag{35}$$

where

$$\begin{aligned} \mathcal{N}^m(\alpha) &:= \left[n^m(\alpha_1), n^m(\alpha_2), n^m(\alpha_3)\right]^T \\ \text{Sig}^q(\alpha) &:= \left[\text{sig}^q(\alpha_1), \text{sig}^q(\alpha_2), \text{sig}^q(\alpha_3)\right]^T \\ \text{sig}^q(\alpha_i) &:= |\alpha_i|^q\text{sgn}(\alpha_i), \ i = 1, 2, 3 \\ n^m(\alpha_i) &:= \begin{cases} ^m(\alpha_i), & |\alpha_i| \geq \varsigma \\ \varsigma^{m-1}\alpha_i, & |\alpha_i| < \varsigma \end{cases} \end{aligned}$$

and the control parameters subject to $\varsigma \in (0, 1]$, $m \in (0, 1), q > 1$. Afterward, the implemented control law is described as

$$\begin{aligned} \tau = 2b_v\left(\ddot{\eta}_d - \dot{\mathcal{D}}e - \mathcal{D}\dot{e}\right) - \hat{\mathcal{A}}(\eta, \dot{\eta}, \ddot{\eta}) - \mathcal{K}_0\text{Sig}^r(s) - b\text{sign}(s) \\ -2b_v\left(\mathcal{C}_1\mathcal{G}^m(\alpha) + q\mathcal{C}_2\mathcal{U}^q(\alpha)\right)\mathcal{W}\beta - \mathcal{K}_t\text{sign}(s) \end{aligned} \tag{36}$$

where

$$\mathcal{G}^m(\alpha) := \text{diag}(g^m(\alpha_1), g^m(\alpha_2), g^m(\alpha_3)) \tag{37}$$

$$\mathcal{U}^q(\alpha) := \text{diag}(|\alpha_1|^{q-1}, |\alpha_2|^{q-1}, |\alpha_3|^{q-1}) \tag{38}$$

$$g^m(\alpha_i) := \begin{cases} m|\alpha_i|^{m-1}, & |\alpha_i| \geq \varsigma \\ \varsigma^{m-1}, & |\alpha_i| < \varsigma \end{cases} \tag{39}$$

$$\text{sign}(s) := \begin{cases} s/\|s\|, & \|s\| \neq 0 \\ 0, & \|s\| = 0 \end{cases} \tag{40}$$

and $b > 0, r > 1, \mathcal{K}_0, \mathcal{C}_1 := \text{diag}(c_{11}, c_{12}, c_{13}), \mathcal{C}_2 := \text{diag}(c_{21}, c_{22}, c_{23})$, and $\mathcal{K}_t$ are parameters tuned carefully to achieve satisfactory performance. From (4), we can obtain $\tau_d = \mathcal{F}^{-1}\tau$. If the vehicle parameters in $\mathcal{F}$ are uncertain, the nominal value of $\mathcal{F}$ can be used for torque transformation in (4) and the corresponding uncertainties can be integrated into the lumped term $\mathcal{O}$ in (9).

Remark 4: The vehicle state information $\eta = [x, y, \phi]^{\text{T}}$ and $\dot{\eta}$, including global position (x, y), yaw angle ϕ, and velocity information, can be obtained for AVs equipped with numerous advanced sensors. The multisensor techniques, such as RTK-GNSS combined with IMU, speedometer, and odometer [42], can provide accurate vehicle state information. Therefore, this article is focused on the integrated controller design for AVs with known state information [43].

D. Main Results

Theorem 1: Given the AVs system (2), (6), and (7) with external disturbance u_{dist} and actuator failures (5), including loss-of-effectiveness faults $\mathcal{L}_a$ and bias faults z_a. The synthesized control scheme (36), with the aid of time-delay information (16) and the bijective error mapping (28), (29), has the capability to guarantee the asymptotic stability of AVs system. In addition, fixed-time convergence to the region $\mathcal{R}_\varsigma := \{\alpha_i \| |\alpha_i| \le \varsigma\}$ of the unconstrained error (30) is assured where the convergence time $\mathcal{T}$ satisfies

$$\mathcal{T} \le \mathcal{B}_1 + \mathcal{B}_2 \tag{41}$$

with

$$\mathcal{B}_1 \le \frac{2\sqrt{b_v}}{b} + \frac{2}{3^{(1-r)/2}(r-1)\lambda_{\min}(\mathcal{K}_0)(b_v)^{2/(r+1)}}$$
$$\mathcal{B}_2 < \frac{1}{(1-m)2^{(m+1)/2}\zeta_{0i}^{-1}c_{1i}} + \frac{1}{2^{(q+1)/2}(q-1)\zeta_{0i}^{-1}c_{2i}}$$

where $\lambda_{\min}(\mathcal{K}_0)$ denotes the minimum eigenvalue of $\mathcal{K}_0$.

Meanwhile, the proposed controller (36) can derive the trajectory tracking error (11) to $(\underline{k}_i\zeta_{\infty i}, \bar{k}_i\zeta_{\infty i})$ within time $\mathcal{S}_i$. Moreover, the transient tracking error $e_i(t)$ is restricted to the established PPFs (22) and (24).

E. Stability Analysis

The Lyapunov function for AVs system (2), (6), and (7) is chosen as

$$\mathcal{V} = \frac{1}{2}s^T\bar{H}s. \tag{42}$$

Accordingly, the derivative of (42) is

$$\dot{\mathcal{V}} = s^T\bar{H}\dot{s}. \tag{43}$$

Combining the designed sliding function (35) and the definitions (37)–(39), one has

$$\dot{s} = \big(\mathcal{C}_1\mathcal{G}^m(\alpha) + q\mathcal{C}_2\mathcal{U}^q(\alpha)\big)\mathcal{W}\beta + \dot{\beta}. \tag{44}$$

By virtue of (33), it follows

$$\begin{aligned}\bar{H}\dot{s} &= \bar{H}\big(\mathcal{C}_1\mathcal{G}^m(\alpha) + q\mathcal{C}_2\mathcal{U}^q(\alpha)\big)\mathcal{W}\beta + \bar{H}\dot{\beta}\\ &= \bar{H}\big(\mathcal{C}_1\mathcal{G}^m(\alpha) + q\mathcal{C}_2\mathcal{U}^q(\alpha)\big)\mathcal{W}\beta + \bar{H}\ddot{\eta}\\ &\quad + \bar{H}\big(-\ddot{\eta}_d + \dot{\mathcal{D}}e + \mathcal{D}\dot{e}\big).\end{aligned} \tag{45}$$

The time-delay information (16) is introduced to estimate the vehicle model, that is,

$$\begin{aligned}\bar{H}\dot{s} = \bar{H}\big(\mathcal{C}_1\mathcal{G}^m(\alpha) + q\mathcal{C}_2\mathcal{U}^q(\alpha)\big)\mathcal{W}\beta + \hat{\mathcal{A}}(\eta,\dot{\eta},\ddot{\eta})\\ + \varrho + \tau + \bar{H}\big(-\ddot{\eta}_d + \dot{\mathcal{D}}e + \mathcal{D}\dot{e}\big).\end{aligned} \tag{46}$$

Substituting the devised control strategy (36)–(46), when $\|s\| \ne 0$, yields

$$\begin{aligned}\bar{H}\dot{s} &= 2b_v\big(\ddot{\eta}_d - \dot{\mathcal{D}}e - \mathcal{D}\dot{e}\big) - \hat{\mathcal{A}}(\eta,\dot{\eta},\ddot{\eta}) - b\frac{s}{\|s\|}\\ &\quad -\mathcal{K}_0\text{Sig}^r(s) - 2b_v\big(\mathcal{C}_1\mathcal{G}^m(\alpha) + q\mathcal{C}_2\mathcal{U}^q(\alpha)\big)\mathcal{W}\beta\\ &\quad + \hat{\mathcal{A}}(\eta,\dot{\eta},\ddot{\eta}) + \varrho + \bar{H}\big(-\ddot{\eta}_d + \dot{\mathcal{D}}e + \mathcal{D}\dot{e}\big)\\ &\quad + \bar{H}\big(\mathcal{C}_1\mathcal{G}^m(\alpha) + q\mathcal{C}_2\mathcal{U}^q(\alpha)\big)\mathcal{W}\beta - \mathcal{K}_t\frac{s}{\|s\|}.\end{aligned} \tag{47}$$

As a consequence, we obtain

$$\bar{H}\dot{s} = -\mathcal{K}_0\text{Sig}^r(s) - b\frac{s}{\|s\|} - \mathcal{K}_t\frac{s}{\|s\|} + \varrho. \tag{48}$$

In this case, (43) can be rewritten as

$$\dot{\mathcal{V}} = -s^T\mathcal{K}_0\text{Sig}^r(s) - s^Tb\frac{s}{\|s\|} + \left\{-\mathcal{K}_t\frac{s^Ts}{\|s\|} + s^T\varrho\right\}. \tag{49}$$

Under Assumption 1 and (20), it holds that

$$\begin{aligned}\dot{\mathcal{V}} &\le -s^T\mathcal{K}_0\text{Sig}^r(s) - s^Tb\frac{s}{\|s\|}\\ &\le -b\left(\frac{1}{b_v}\right)^{\frac{1}{2}}\mathcal{V}^{\frac{1}{2}} - \lambda_{\min}(\mathcal{K}_0)\sum_{i=1}^{3}|s_i|^{r+1}.\end{aligned} \tag{50}$$

On account of Lemma 1, we have

$$\begin{aligned}\dot{\mathcal{V}} &\le \frac{-b}{\sqrt{b_v}}\mathcal{V}^{\frac{1}{2}} - 3^{\frac{1-r}{2}}\lambda_{\min}(\mathcal{K}_0)\|s\|^{r+1}\\ &\le -b\big(s^Ts\big)^{\frac{1}{2}} - 3^{\frac{1-r}{2}}\lambda_{\min}(\mathcal{K}_0)\|s\|^{r+1}\end{aligned} \tag{51}$$

which is equivalent to

$$\dot{\mathcal{V}} + \varepsilon_1\mathcal{V}^{\frac{1}{2}} + \varepsilon_2\mathcal{V}^{\frac{r+1}{2}} \le 0 \tag{52}$$

where $\varepsilon_1 := (b/(b_v)^{1/2})$ and $\varepsilon_2 := 3^{(1-r/2)}\lambda_{\min}(\mathcal{K}_0)(b_v)^{(2/r+1)}$. Invoking Lemma 2, the convergence time $\mathcal{B}_1$ satisfies

$$\mathcal{B}_1 \le \frac{2}{\varepsilon_1} + \frac{2}{\varepsilon_2(r-1)}. \tag{53}$$

Therefore, for $t > \mathcal{B}_1$, we get $\mathcal{C}_1\mathcal{N}^m(\alpha) + \mathcal{C}_2\text{Sig}^q(\alpha) + \beta = 0$, which implies that $\beta_i = -c_{1i}n^m(\alpha_i) - c_{2i}\text{sig}^q(\alpha_i)$.

Consider the following Lyapunov function:

$$\mathcal{I} = \frac{1}{2}\alpha_i^2. \tag{54}$$

If the transformed error α_i reaches the prescribed neighborhood ς, then one can obtain $\beta_i = -\varsigma^{m-1}c_{1i}\alpha_i - c_{2i}\text{sig}^q(\alpha_i)$, which results in the derivative of (54) as

$$\begin{aligned}\dot{\mathcal{I}} &= \varpi_i\alpha_i\big\{-\varsigma^{m-1}c_{1i}\alpha_i - c_{2i}\text{sig}^q(\alpha_i)\big\}\\ &= -\varsigma^{m-1}c_{1i}\varpi_i\alpha_i^2 - c_{2i}\varpi_i|\alpha_i|^{q+1}.\end{aligned} \tag{55}$$

Recall that $c_{1i}, c_{2i}, \varpi_i, \varsigma^{m-1} > 0$, and $\dot{\mathcal{I}} < 0$ holds. The asymptotic convergence of transformed error α_i is proved. For α_i outside the prescribed error region, which means that $|\alpha_i| \ge \varsigma$, then $\beta_i = -c_{1i}\text{sig}^m(\alpha_i) - c_{2i}\text{sig}^q(\alpha_i)$.

Subsequently, the derivative of (54) yields

$$\begin{aligned}\dot{\mathcal{I}} &= \varpi_i\alpha_i\big\{-c_{1i}\ \text{sig}^m(\alpha_i) - c_{2i}\text{sig}^q(\alpha_i)\big\}\\ &= -\varpi_ic_{1i}|\alpha_i|^{m+1} - \varpi_ic_{2i}|\alpha_i|^{q+1}.\end{aligned} \tag{56}$$

From (22) and (32), one obtains $\varpi_i > (2/\zeta_i) > 2\zeta_{0i}^{-1}$. Consequently

$$\begin{aligned}\dot{\mathcal{I}} &< -2\zeta_{0i}^{-1}c_{1i}|\alpha_i|^{m+1} - 2\zeta_{0i}^{-1}c_{2i}|\alpha_i|^{q+1}\\ &< -2^{\frac{m+3}{2}}\zeta_{0i}^{-1}c_{1i}(\mathcal{I})^{\frac{m+1}{2}} - 2^{\frac{q+3}{2}}\zeta_{0i}^{-1}c_{2i}(\mathcal{I})^{\frac{q+1}{2}}\end{aligned} \tag{57}$$

which leads to

$$\dot{\mathcal{I}} + 2^{\frac{m+3}{2}}\zeta_{0i}^{-1}c_{1i}(\mathcal{I})^{\frac{m+1}{2}} + 2^{\frac{q+3}{2}}\zeta_{0i}^{-1}c_{2i}(\mathcal{I})^{\frac{q+1}{2}} < 0. \tag{58}$$

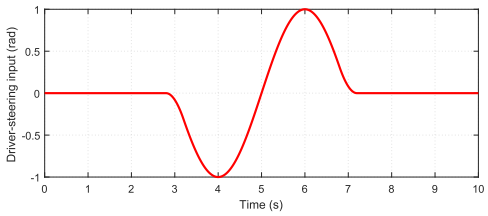

Fig. 3. Input steering wheel angle for single-lane change scenario.

Using Lemma 2, one concludes that steers α_i to $\mathcal{R}_\varsigma := \{\alpha_i \| \alpha_i| \leq \varsigma\}$ within a fixed time $\mathcal{B}_2$, which is bounded by

$$\mathcal{B}_2 < \frac{1}{2^{\frac{m+1}{2}}\zeta_{0i}^{-1}c_{1i}(1-m)} + \frac{1}{2^{\frac{q+1}{2}}\zeta_{0i}^{-1}c_{2i}(q-1)}. \quad (59)$$

Therefore, the stability is proved as above. According to the error transformation $e_i = \zeta_i \sigma^{-1}(\alpha_i)$, $\sigma^{-1}(0) = 0$, we can have $e_i \in (\underline{k}_i\zeta_i, \bar{k}_i\zeta_i)$ when $\sigma^{-1}(\alpha_i) \in (\underline{k}_i, \bar{k}_i)$, which implies (41) holds.

Remark 5: The controller parameters $\zeta_{\infty i}$, ζ_{0i}, μ_i, $\mathcal{S}_i$, and p_i, $i = 1, 2, 3$ depend on the desired prescribed performance constraints, which determine the final properties of the PPF and satisfy $|e_i(0)| \in (\zeta_{\infty i}, \zeta_{0i})$, $\mu_i \in (0, 1)$, $\mathcal{S}_i > 0$, and $p_i > 1$. Moreover, to attain fixed-time convergence property, the parameters subject to $\varsigma \in (0, 1], m \in (0, 1)$, and $q > 1$. The parameters mentioned above determine the constraint settings of the tracking errors and the convergence properties of the slide mode surface. Meanwhile, $b > 0$, $r > 1, \mathcal{K}_0, \mathcal{C}_1 := \text{diag}(c_{11}, c_{12}, c_{13})$, $\mathcal{C}_2 := \text{diag}(c_{21}, c_{22}, c_{23})$, and $\mathcal{K}_t$ are tuned carefully by numerous trial-and-error simulations to achieve satisfactory performance.

Remark 6: This article proposed a novel integrated motion controller to handle the subsystems' interactions and strong coupling with time-varying longitudinal velocity. Meanwhile, the unknown disturbance and actuator faults are addressed by embedding TDE without the need for additional information. The reference dynamics and trajectory can be tracked accurately with the presented control framework, and the robustness and reliability are enhanced significantly.

IV. Simulation Analysis

Aiming to demonstrate the feasibility and superiority of the proposed prescribed performance integrated control strategy (PPIC), simulation comparisons with vehicle IMC [9], the classical NSTM [15], and nonsingular fast terminal sliding-mode (NFTSM) [14], in single-lane change and J-turn testing scenarios, and polynomial planning maneuver for the 7-DOF vehicle model (2), (6), and (7) are performed in this section.

A. Single-Lane Change Maneuver

The desired steering wheel angle for single-lane maneuver is illustrated in Fig. 3. The controller parameters are $\mu_i = 0.6, p_i = 2.2, \mathcal{S}_i = 2, i = 1, 2, 3$, $\zeta_{01} = 0.4$, $\zeta_{02} = 0.4, \zeta_{03} = 0.1, \zeta_{\infty 1} = 0.005, \zeta_{\infty 2} = 0.01, \zeta_{\infty 3} = 0.005$, $q = 1.4, m = 0.6, r = 1.4, \varsigma = 0.001$, $\mathcal{K}_0 = \text{diag}(0.1, 50, 0.45), \mathcal{C}_1 = 10^{-2}\cdot\text{diag}(1, 1, 1), \mathcal{C}_2 = 0.01 \cdot \text{diag}(1, 3, 0.01), b_v = 0.5, b = 0.001$, and

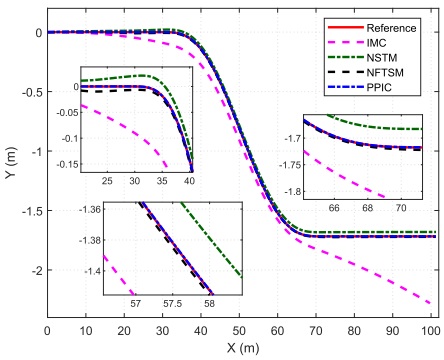

Fig. 4. IMC overall performance.

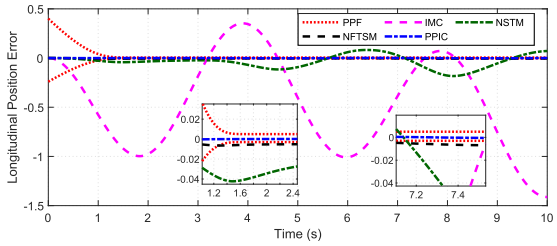

Fig. 5. Longitudinal position tracking error in the global coordinate frame.

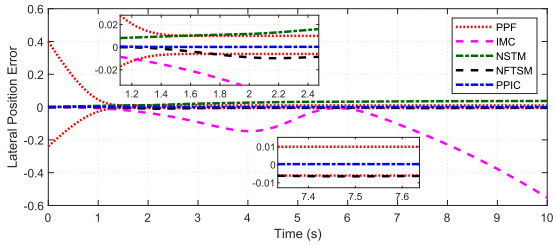

Fig. 6. Lateral position tracking error in the global coordinate frame.

$\mathcal{K}_t = \text{diag}(5, 0.26, 0.3)$. Meanwhile, the external disturbance vector u_{dist} in (7) is set as $u_{\text{dist}} = [4\cos(0.1t - (\pi/3)), 3\cos(0.1t + (\pi/6)), 0.01\cos(0.1t - (\pi/4))]^{\text{T}}$ to verify the robustness of the proposed PPIC. Moreover, the time-varying actuator failures in (5) are chosen as

$$z_{a1}(t), \ell_{a1}(t) = \begin{cases} 0, & (t < 4) \\ 0.7 + 0.05 \cdot \sin(0.25t), & (4 \leq t \leq 10) \end{cases}$$

$$z_{a2}(t), \ell_{a2}(t) = \begin{cases} 0, & (t < 3) \\ 0.8 + 0.05 \cdot \sin(0.25t), & (3 \leq t \leq 10) \end{cases}$$

$$\ell_{a3}(t) = \begin{cases} 0, & (t < 2) \\ 0.95 + 0.05 \cdot \sin(0.25t), & (2 \leq t \leq 10) \end{cases}$$

$$z_{a3}(t) = \begin{cases} 0, & (t < 2) \\ 0.05 \cdot \sin(0.25t), & (2 \leq t \leq 10). \end{cases}$$

The overall performance of the designed integrated motion controller is illustrated in Fig. 4. The longitudinal position, lateral position, and yaw angle tracking error in the global coordinate frame are depicted in Figs. 5–7, respectively. Although the pioneering NSTM has addressed the singularity problem effectively and enhanced the robustness

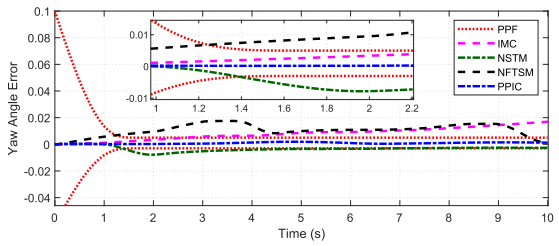

Fig. 7. Yaw angle tracking error.

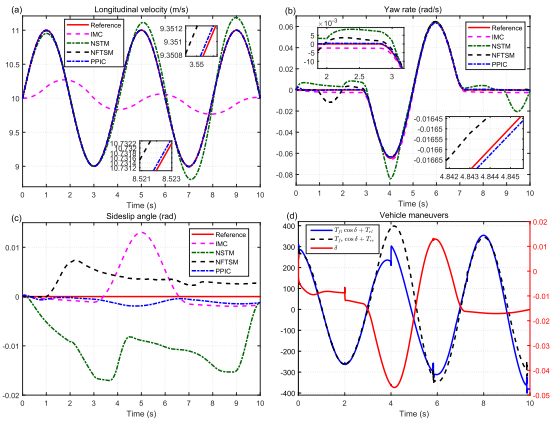

Fig. 8. Performance comparisons and vehicle maneuvers. (a) Longitudinal velocity tracking performance comparison. (b) Yaw rate tracking performance comparison. (c) Vehicle sideslip angle. (d) Vehicle maneuvers.

to disturbances, performance degrades when actuator failures occur. The IMC attempts to address the longitudinal and lateral subsystems simultaneously with integrated control technique. Nevertheless, the trajectory tracking performance with the time-varying longitudinal velocity and actuator faults is unsatisfactory. The classical NSTM and NFTSM obtain higher trajectory tracking performance than IMC, shown in Fig. 4. NFTSM is capable of handling the actuator failures; however, additional knowledge is required. By contrast, the proposed PPIC enhances the tracking performance significantly where the transient response is confined within the constructed PPF.

As illustrated in Fig. 8, the performance comparison and vehicle maneuvers are provided for further analysis. Superior longitudinal velocity tracking performance and stability are achieved by the NFTSM than NSTM and IMC, as displayed in Fig. 8(a) and (c). Conversely, vehicle handling is optimized through the IMC in Fig. 8(b). Meanwhile, the vehicle maneuvers are shown in Fig. 8(d). Compared to these approaches, the designed PPIC improves the overall performance considerably, involving trajectory tracking performance, longitudinal velocity tracking performance, handling, and stability.

B. J-Turn Maneuver

Fig. 9 shows the steering wheel angle input for J-turn maneuver. Correspondingly, the exactly same controller parameters, external disturbances, and actuator failures as single-lane change maneuver are chosen.

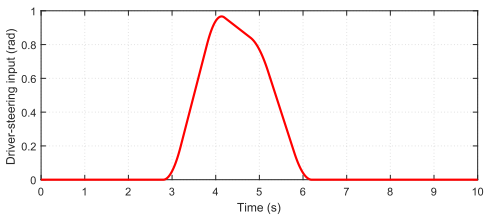

Fig. 9. Input steering wheel angle for J-turn scenario.

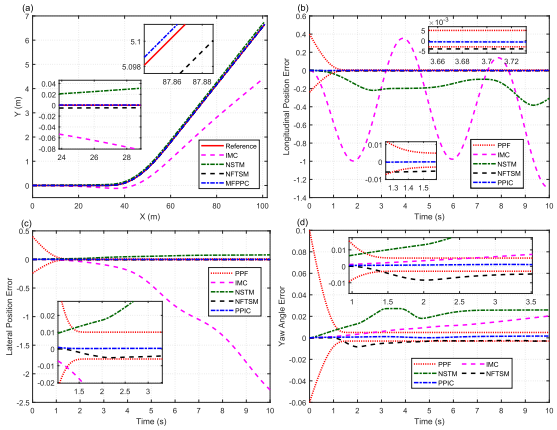

Fig. 10. IMC performance in the global coordinate frame for J-turn scenario. (a) Overall performance. (b) Longitudinal position tracking error. (c) Lateral position tracking error. (d) Yaw angle tracking error.

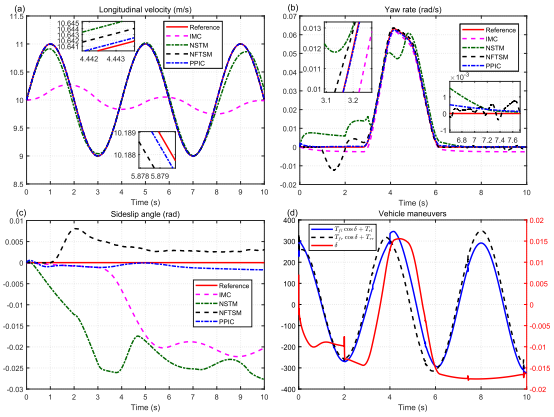

Fig. 11. Performance comparisons and vehicle maneuvers for J-turn scenario. (a) Longitudinal velocity tracking performance comparison. (b) Yaw rate tracking performance comparison. (c) Vehicle sideslip angle. (d) Vehicle maneuvers.

The trajectory tracking performance for J-turn maneuver can be seen in Fig. 10. The constructed PPIC control scheme illustrated in Fig. 2 is able to ensure that the trajectory tracking errors satisfy the PPF transient behavior constraints (22)–(25) by the error mapping (28). The trajectory tracking performance in Fig. 10(a) demonstrates the overall performance enhancement attained by the proposed PPIC intuitively. In comparison with the innovative work NSTM and NFTSM, the robustness against external disturbances and actuator failures is further improved. Meanwhile, the superior yaw angle tracking performance than IMC is obtained.

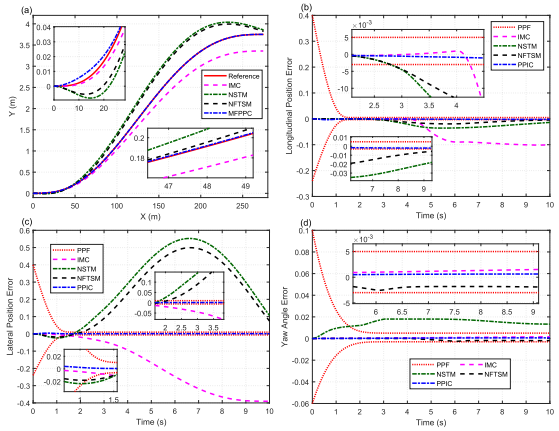

Fig. 12. Polynomial planning maneuver performance. (a) Overall performance. (b) Longitudinal position tracking error. (c) Lateral position tracking error. (d) Yaw angle tracking error.

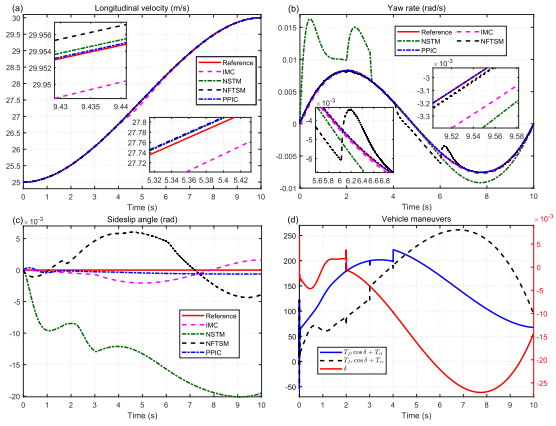

Fig. 13. Performance comparisons and vehicle maneuvers for polynomial planning scenario. (a) Longitudinal velocity tracking performance. (b) Yaw rate tracking performance. (c) Vehicle sideslip angle. (d) Vehicle maneuvers.

The detailed performance comparison and vehicle maneuvers for J-turn maneuver are plotted in Fig. 11. As diagrammed in Fig. 11(a) and (b), the reference time-varying longitudinal velocity can be tracked accurately and the resulting strong couplings and interactions are handled effectively. The corresponding vehicle maneuvers are provided in Fig. 11(d). Additionally, the significant vehicle handling and stability improvement can be observed in Fig. 11(b) and (c).

C. Polynomial Planning Maneuver

A time-dependent polynomial trajectory is introduced in this section to verify the effectiveness of the designed controller. Unlike the J-turn and single-lane change maneuvers, the time-dependent trajectory is generated by the upper-level motion planning to achieve safe lateral collision avoidance, as detailed in [32]. Meanwhile, the same controller parameters, external disturbances, and actuator failures as single-lane change maneuver are chosen. Different from the IMC, (12) and (13) are not required for the planned trajectory. The corresponding trajectory with lane-change time $t_l = 10$ s, initial longitudinal vehicle velocity $v_0 = 25$ m/s, and target velocity $v_t = 30$ m/s can be expressed as

$$\begin{cases} x_d(t) = p_0 + p_1 t + p_2 t^2 + p_3 t^3 + p_4 t^4 + p_5 t^5 \\ y_d(t) = q_0 + q_1 t + q_2 t^2 + q_3 t^3 + q_4 t^4 + q_5 t^5 \end{cases}$$

where the trajectory parameters are set as $p_0 = p_2 = p_5 = 0$, $p_1 = 25$, $p_3 = (5/{t_l}^2)$, $p_4 = -(2.5/{t_l}^3)$, $q_0 = q_1 = q_2 = 0$, $q_3 = (37.5/{t_l}^3)$, $q_4 = -(56.25/{t_l}^4)$, $q_5 = (112.5/{t_l}^5)$.

The overall tracking performance of the polynomial safe planned trajectory considering lateral collision avoidance is shown in Fig. 12(a). The longitudinal position, lateral position, and yaw angle tracking errors are depicted in Fig. 12(b)–(d), respectively. As it can be noticed, compared with NSTM [15], NFTSM [14], and IMC [9], significant overall tracking performance improvement is achieved by the proposed control scheme. In particular, the lateral position tracking performance in high longitudinal speed with the increased lateral-longitudinal coupling is enhanced significantly. Meanwhile, the designed prescribed performance constraints are satisfied.

Fig. 13(a) demonstrates the longitudinal velocity tracking performance improvement. The corresponding vehicle maneuvers are shown in Fig. 13(d). It can be observed that the proposed controller achieves satisfactory control performance in the presence of unknown time-varying actuator faults and disturbances. In addition, as visualized in Fig. 13(b), the yaw rate tracking performance comparable to IMC [9] is obtained, which implies superior vehicle handling. Also, the stability enhancement can be clearly seen from the vehicle sideslip angle in Fig. 13(c).

Remark 7: It is worth mentioning that the total simulation time of the above scenarios in MATLAB 2021a is about 1.5–1.9 s with Intel Core i7-10700 K CPU @ 3.80 GHz and 16.0-GB RAM. The computational time of the proposed control method is feasible and acceptable in practice.

Remark 8: From (36), it is clear that the designed controller contains only the TDE information, the vehicle state information, and the corresponding reference values, as well as the controller parameters. This means that controller stability and robustness can be guaranteed by employing the designed controller under model uncertainties, parameter uncertainties, and various road conditions. Vertical motion is neglected in this article; however, the vehicle-IMC further considering roll, pitch, and vertical dynamics is an interesting and more challenging topic. Addressing the lateral, longitudinal, and vertical vehicle dynamics couplings and interactions by employing time-delay information or NN to obtain superior tracking performance, ride comfort, stability, and handling is the focus of our future work.

D. Quantitative Results

For the purpose of evaluating the performance of PPIC quantitatively, root mean square (rms) is introduced as performance index in this section. The rms value of the signal $\varkappa(t)$ is given by $\text{rms}_\varkappa = ((1/\mathcal{H}) \int_0^{\mathcal{H}} \varkappa^T(t)\varkappa(t)dt)^{1/2}$, where $\mathcal{H}$ denotes the time duration of the signal $\varkappa(t)$. The simulation time duration of each signal for single-lane change and

TABLE II
RMS OF VEHICLE STATES IN SINGLE-LANE CHANGE MANEUVER

Term	IMC	NSTM	NFTSM	PPIC
e_x	0.6606	0.0742	**0.0046**	**1.00E-03 (↓ 78.26%)**
e_y	0.1953	0.0282	**0.0049**	**5.63E-04 (↓ 88.5%)**
e_{v_x}	0.7008	0.1126	**0.0032**	**0.0011 (↓ 65.63%)**
e_ω	**1.90E-03**	0.007	2.90E-03	**6.54E-04 (↓ 65.59%)**
β_v	0.0049	0.0111	**0.0038**	**0.0011 (↓ 71.05%)**

TABLE III
RMS OF VEHICLE STATES IN J-TURN MANEUVER

Term	IMC	NSTM	NFTSM	PPIC
e_x	0.6301	0.1943	**0.0035**	**9.01E-04 (↓ 74.25%)**
e_y	0.9769	0.0561	**0.0034**	**7.17E-04 (↓ 78.92%)**
e_{v_x}	0.7046	0.0968	**0.0022**	**0.001 (↓ 54.55%)**
e_ω	**2.10E-03**	0.0064	3.20E-03	**4.79E-04 (↓ 77.19%)**
β_v	0.015	0.0209	**0.0039**	**0.001 (↓ 74.36%)**

TABLE IV
RMS OF VEHICLE STATES IN POLYNOMIAL PLANNING MANEUVER

Term	IMC	NSTM	NFTSM	PPIC
e_x	0.066	0.0226	**0.0113**	**1.20E-03 (↓ 89.38%)**
e_y	**0.2372**	0.3455	0.3041	**1.50E-03 (↓ 99%)**
e_{v_x}	0.0234	0.0063	**0.0075**	**0.0052 (↓ 30.67%)**
e_ω	**1.68E-04**	0.0038	6.58E-04	**1.86E-04 (↓ 10%)**
β_v	0.0012	0.0148	**0.0038**	**0.001 (↓ 73.68%)**

J-turn testing maneuvers is 10 s. The rms value of longitudinal position tracking error e_x, lateral position tracking error e_y, longitudinal velocity tracking error e_{v_x}, yaw rate tracking error e_ω, and vehicle sideslip angle β_v are calculated and provided to evaluate the overall performance.

As detailed in Tables II–IV, IMC, NFTSM, the classical NSTM, and the constructed PPIC are performed in the single-lane change maneuver and J-turn maneuver, and polynomial planning maneuver. The optimal and suboptimal performance is bolded, while the error percentage reductions are calculated and added to the tables. The overall performance improvement is validated through considerable trajectory tracking errors e_x, e_y reduction (over 70%). Longitudinal velocity v_x can be tracked precisely with a substantial reduction of e_{v_x} (over 30%) which means that the strong couplings and interactions are tackled adequately. Meanwhile, the sizeable decrease of yaw rate tracking error e_ω (dropped over 10%) and vehicle sideslip angle β_v (dropped over 70%) corroborates the benefits in handling and stability of the proposed PPIC, respectively.

V. CONCLUSION

The strong couplings and interactions between longitudinal and lateral subsystems and the resulting nonlinearities for vehicle model motivate the work in this article, which leverages time-delay information to remove the need for complex dynamics relationships. A distinguishing feature of the presented integrated control framework is the transient behavior constraints with fixed-time convergence property can be satisfied. Moreover, the robustness is increased by taking external disturbance and actuator faults into consideration. Comparative simulation results in standard testing maneuvers and polynomial planning scenario demonstrate that tracking performance, handling, and stability are improved significantly. Quantitatively, compared to the optimal performance in IMC, NFTSM, and NSTM, the position and longitudinal velocity tracking error of the proposed PPIC reduced by over 70% and 30%. Meanwhile, the reductions in the yaw rate tracking error (over 10%) and vehicle sideslip angles (over 70%) demonstrate further improvements in vehicle handling and stability, respectively.

Future work involves improving the designed control scheme to obtain better convergence properties and verifying by experimental work. Moreover, IMC which takes ride comfort into account, including the longitudinal, lateral, and vertical subsystems, will be further investigated.

REFERENCES

[1] W. Wei, S. Ramakrishnan, Z. A. Needell, and J. E. Trancik, "Personal vehicle electrification and charging solutions for high-energy days," *Nature Energy*, vol. 6, no. 1, pp. 105–114, Jan. 2021.
[2] M. Boujelben and R. Trigui, "Optimal power control for a variable-speed generator integrated in series hybrid vehicle," *IEEE Trans. Transport. Electrific.*, vol. 8, no. 1, pp. 1302–1312, Mar. 2022.
[3] S. Geller, I. Avrahami, and N. Shvalb, "Control of autonomous vehicles flow using imposed speed profiles," *J. Intell. Transp. Syst.*, vol. 26, no. 5, pp. 529–543, Sep. 2022.
[4] K. P. Divakarla, A. Emadi, and S. Razavi, "A cognitive advanced driver assistance systems architecture for autonomous-capable electrified vehicles," *IEEE Trans. Transport. Electrific.*, vol. 5, no. 1, pp. 48–58, Mar. 2019.
[5] H. Pan, Y. Hong, W. Sun, and Y. Jia, "Deep dual-resolution networks for real-time and accurate semantic segmentation of traffic scenes," *IEEE Trans. Intell. Transp. Syst.*, early access, Dec. 21, 2022, doi: 10.1109/TITS.2022.3228042.
[6] W. Wang, T. Ma, C. Yang, Y. Zhang, Y. Li, and T. Qie, "A path following lateral control scheme for four-wheel independent drive autonomous vehicle using sliding mode prediction control," *IEEE Trans. Transport. Electrific.*, vol. 8, no. 3, pp. 3192–3207, Sep. 2022.
[7] W. Sun, J. Zhang, and Z. Liu, "Two-time-scale redesign for antilock braking systems of ground vehicles," *IEEE Trans. Ind. Electron.*, vol. 66, no. 6, pp. 4577–4586, Jun. 2019.
[8] P. Hang, X. Xia, and X. Chen, "Handling stability advancement with 4WS and DYC coordinated control: A gain-scheduled robust control approach," *IEEE Trans. Veh. Technol.*, vol. 70, no. 4, pp. 3164–3174, Apr. 2021.
[9] J. Zhang, W. Sun, and H. Du, "Integrated motion control scheme for four-wheel-independent vehicles considering critical conditions," *IEEE Trans. Veh. Technol.*, vol. 68, no. 8, pp. 7488–7497, Aug. 2019.
[10] H. Pan, H. Li, W. Sun, and Z. Wang, "Adaptive fault-tolerant compensation control and its application to nonlinear suspension systems," *IEEE Trans. Syst., Man, Cybern. Syst.*, vol. 50, no. 5, pp. 1766–1776, May 2020.
[11] E. Ono, Y. Hattori, Y. Muragishi, and K. Koibuchi, "Vehicle dynamics integrated control for four-wheel-distributed steering and four-wheel-distributed traction/braking systems," *Vehicle Syst. Dyn., Int. J. Vehicle Mech. Mobility*, vol. 44, no. 2, pp. 139–151, 2006.
[12] R. Tchamna and I. Youn, "Yaw rate and side-slip control considering vehicle longitudinal dynamics," *Int. J. Automot. Technol.*, vol. 14, no. 1, pp. 53–60, 2013.
[13] N. Ahmadian, A. Khosravi, and P. Sarhadi, "Driver assistant yaw stability control via integration of AFS and DYC," *Vehicle Syst. Dyn.*, vol. 60, no. 5, pp. 1742–1762, Jun. 2021.
[14] S. S. D. Xu, C. C. Chen, and Z. L. Wu, "Study of nonsingular fast terminal sliding-mode fault-tolerant control," *IEEE Trans. Ind. Electron.*, vol. 62, no. 6, pp. 3906–3913, Jun. 2015.
[15] Y. Feng, X. Yu, and F. Han, "On nonsingular terminal sliding-mode control of nonlinear systems," *Automatica*, vol. 49, no. 6, pp. 1715–1722, 2013.
[16] A. Polyakov, D. Efimov, and W. Perruquetti, "Finite-time and fixed-time stabilization: Implicit Lyapunov function approach," *Automatica*, vol. 51, pp. 332–340, Jan. 2015.

[17] J. Wang, H. Pan, and W. Sun, "Event-triggered adaptive fault-tolerant control for unknown nonlinear systems with applications to linear motor," *IEEE/ASME Trans. Mechatronics*, vol. 27, no. 2, pp. 940–949, Apr. 2022.

[18] K. Shojaei, "A prescribed performance PID control of robotic cars with only posture measurements considering path curvature," *Eur. J. Control*, vol. 65, May 2022, Art. no. 100616.

[19] P. Yang and Y. Su, "Proximate fixed-time prescribed performance tracking control of uncertain robot manipulators," *IEEE/ASME Trans. Mechatronics*, vol. 27, no. 5, pp. 3275–3285, Oct. 2022.

[20] H. Pan, C. Zhang, and W. Sun, "Fault-tolerant multiplayer tracking control for autonomous vehicle via model-free adaptive dynamic programming," *IEEE Trans. Rel.*, early access, Sep. 30, 2022, doi: 10.1109/TR.2022.3208467.

[21] W. Sun, X. Wang, and C. Zhang, "A model-free control strategy for vehicle lateral stability with adaptive dynamic programming," *IEEE Trans. Ind. Electron.*, vol. 67, no. 12, pp. 10693–10701, Dec. 2020.

[22] M. Jin, J. Lee, P. H. Chang, and C. Choi, "Practical nonsingular terminal sliding-mode control of robot manipulators for high-accuracy tracking control," *IEEE Trans. Ind. Electron.*, vol. 56, no. 9, pp. 3593–3601, Sep. 2009.

[23] H. Tang, Y. Chen, and A. Zhou, "Actuator fault-tolerant control for four-wheel-drive-by-wire electric vehicle," *IEEE Trans. Transport. Electrific.*, vol. 8, no. 2, pp. 2361–2373, Jun. 2022.

[24] N. Guo, X. Zhang, Y. Zou, B. Lenzo, G. Du, and T. Zhang, "A supervisory control strategy of distributed drive electric vehicles for coordinating handling, lateral stability, and energy efficiency," *IEEE Trans. Transport. Electrific.*, vol. 7, no. 4, pp. 2488–2504, Dec. 2021.

[25] A. P. Aguiar and J. P. Hespanha, "Trajectory-tracking and path-following of underactuated autonomous vehicles with parametric modeling uncertainty," *IEEE Trans. Autom. Control*, vol. 52, no. 8, pp. 1362–1379, Aug. 2007.

[26] M. A. Djeziri, R. Merzouki, B. O. Bouamama, and M. Ouladsine, "Fault diagnosis and fault-tolerant control of an electric vehicle overactuated," *IEEE Trans. Veh. Technol.*, vol. 62, no. 3, pp. 986–994, Mar. 2013.

[27] T. Stolte, "Actuator fault-tolerant vehicle motion control: A survey," 2021, *arXiv:2103.13671*.

[28] H. Pan, D. Zhang, W. Sun, and X. Yu, "Event-triggered adaptive asymptotic tracking control of uncertain MIMO nonlinear systems with actuator faults," *IEEE Trans. Cybern.*, vol. 52, no. 9, pp. 8655–8667, Sep. 2022.

[29] C. Hu, R. Wang, F. Yan, and N. Chen, "Robust composite nonlinear feedback path-following control for underactuated surface vessels with desired-heading amendment," *IEEE Trans. Ind. Electron.*, vol. 63, no. 10, pp. 6386–6394, Oct. 2016.

[30] K. Shojaei, "Neural adaptive PID formation control of car-like mobile robots without velocity measurements," *Adv. Robot.*, vol. 31, no. 18, pp. 947–964, 2017.

[31] M. Van, S. S. Ge, and H. Ren, "Finite time fault tolerant control for robot manipulators using time delay estimation and continuous nonsingular fast terminal sliding mode control," *IEEE Trans. Cybern.*, vol. 47, no. 7, pp. 1681–1693, Jul. 2017.

[32] X. Li, Z. Guo, D. Su, and Q. Liu, "Time-dependent lane change trajectory optimisation considering comfort and efficiency for lateral collision avoidance," *IET Intell. Transp. Syst.*, vol. 15, no. 5, pp. 595–605, May 2021.

[33] R. N. Jazar, *Vehicle Dynamics: Theory and Application*. Berlin, Germany: Springer, 2017.

[34] P. Wang, H. Liu, L. Guo, L. Zhang, H. Ding, and H. Chen, "Design and experimental verification of real-time nonlinear predictive controller for improving the stability of production vehicles," *IEEE Trans. Control Syst. Technol.*, vol. 29, no. 5, pp. 2206–2213, Sep. 2020.

[35] T. Huang, H. Pan, W. Sun, and H. Gao, "Sine resistance network-based motion planning approach for autonomous electric vehicles in dynamic environments," *IEEE Trans. Transport. Electrific.*, vol. 8, no. 2, pp. 2862–2873, Jun. 2022.

[36] L. Cai and J. Yang, "Asymptotic stability of electric-vehicle-to-grid system with actuator faults," *IEEE Trans. Transport. Electrific.*, vol. 7, no. 4, pp. 2439–2452, Dec. 2021.

[37] X. Cao, Y. Tian, X. Ji, and B. Qiu, "Fault-tolerant controller design for path following of the autonomous vehicle under the faults in braking actuators," *IEEE Trans. Transport. Electrific.*, vol. 7, no. 4, pp. 2530–2540, Dec. 2021.

[38] R. Wang, H. Zhang, and J. Wang, "Linear parameter-varying controller design for four-wheel independently actuated electric ground vehicles with active steering systems," *IEEE Trans. Control Syst. Technol.*, vol. 22, no. 4, pp. 1281–1296, Jul. 2014.

[39] G. H. Hardy, J. E. Littlewood, G. Polya, and G. Polya, *Inequalities*. Cambridge, U.K.: Cambridge Univ. Press, 1952.

[40] A. Polyakov, "Nonlinear feedback design for fixed-time stabilization of linear control systems," *IEEE Trans. Autom. Control*, vol. 57, no. 8, pp. 2106–2110, Aug. 2012.

[41] J. Lee, P. H. Chang, and M. Jin, "An adaptive gain dynamics for time delay control improves accuracy and robustness to significant payload changes for robots," *IEEE Trans. Ind. Electron.*, vol. 67, no. 4, pp. 3076–3085, Apr. 2020.

[42] A. El-Mowafy and N. Kubo, "Integrity monitoring for positioning of intelligent transport systems using integrated RTK-GNSS, IMU and vehicle odometer," *IET Intell. Transp. Syst.*, vol. 12, no. 8, pp. 901–908, 2018.

[43] A.-A. Mamun, Z. Liu, D. M. Rizzo, and S. Onori, "An integrated design and control optimization framework for hybrid military vehicle using lithium-ion battery and supercapacitor as energy storage devices," *IEEE Trans. Transport. Electrific.*, vol. 5, no. 1, pp. 239–251, Mar. 2019.

Tenglong Huang received the B.E. degree in automation from the Henan University of Technology, Zhengzhou, China, in 2019. He is currently pursuing the Ph.D. degree with the Research Institute of Intelligent Control and Systems, Harbin Institute of Technology, Harbin, China.

His current research interests include motion planning, vehicle dynamics control, adaptive control, and fault-tolerant control.

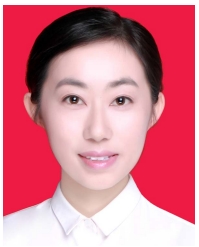

Jue Wang received the B.S. degree in automation and the M.S. degree in pattern recognition and intelligent system from Huaqiao University, Xiamen, China, in 2016 and 2019, respectively. She is currently pursuing the Ph.D. degree with the Research Institute of Intelligent Control and Systems, Harbin Institute of Technology, Harbin, China.

Her current research interests include adaptive control, fault-tolerant control, and intelligent vehicles.

Huihui Pan (Member, IEEE) received the Ph.D. degree in control science and engineering from the Harbin Institute of Technology, Harbin, China, in 2017, and the Ph.D. degree in mechanical engineering from The Hong Kong Polytechnic University, Hong Kong, in 2018.

Since December 2017, he has been with the Research Institute of Intelligent Control and Systems, Harbin Institute of Technology. His research interests include nonlinear control, vehicle dynamic control, and intelligent vehicles.

Dr. Pan is an Associate Editor of IEEE TRANSACTIONS ON INTELLIGENT VEHICLES and *Mechatronics*.

Weichao Sun (Senior Member, IEEE) received the Ph.D. degree in control science and engineering from the Harbin Institute of Technology, Harbin, China, in 2013.

He is currently a Professor with the Research Institute of Intelligent Control Systems, Harbin Institute of Technology. His research interests include adaptive robust control, mechatronics, robotics, and autonomous vehicles.

Dr. Sun is an Associate Editor of the IEEE TRANSACTIONS ON SYSTEMS, MAN, AND CYBERNETICS: SYSTEMS, *Mechatronics*, and the *Journal of Dynamic Systems, Measurement, and Control*.